J. Fluid Mech. (1994), *vol.* 263, *pp.* 293–318

On the three-dimensional internal waves excited by topography in the flow of a stratified fluid

By HIDESHI HANAZAKI

National Institute for Environmental Studies, Tsukuba, Ibaraki 305, Japan

(Received 22 December 1992 and in revised form 12 September 1993)

A numerical study of the three-dimensional internal waves excited by topography in the flow of a stratified fluid is described. In the resonant flow of a nearly two-layer fluid, it is found that the time-development of the nonlinearly excited waves agrees qualitatively with the solution of the forced KP equation or the forced extended KP equation. In this case, the upstream-advancing solitary waves become asymptotically straight crested because of abnormal reflection at the sidewall similar to Mach reflection. The same phenomenon also occurs in the subcritical flow of a nearly two-layer fluid. However, in the subcritical flow of a linearly stratified Boussinesq fluid, the two-dimensionalization of the upstream waves can be interpreted as the separation of the lateral modes due to the differences in the group velocity of the linear wave, although this does not mean in general that the generation of upstream waves is describable by the linearized equation.

1. Introduction

Recent studies on the waves excited by an obstacle in a flow have revealed the basic nonlinear wave-generation mechanism. The mechanism is now found to be essentially the same for water waves, internal gravity waves in stratified flows and inertial waves in swirling flows.

To describe two-dimensional nonlinear water waves, the forced Boussinesq equations (Wu 1981), the Green–Naghdi (GN) equations (Green & Naghdi 1976*a*, *b*) and the forced Korteweg–de Vries (fKdV) equation (Akylas 1984) have been derived. Their applicability has been verified experimentally by Ertekin (1984), Ertekin, Webster & Wehausen (1984) and Lee, Yates & Wu (1989) among others.

For two-dimensional internal waves in stratified flows Grimshaw & Smyth (1986) derived the fKdV equation. In experiments and numerical studies of two-layer flow, Zhu, Wu & Yates (1986, 1987) and Melville & Helfrich (1987) found that the fKdV equation is qualitatively applicable to two-layer flow in that it predicts the existence of upstream-advancing waves near resonance. However, they noticed that the upstream-advancing speed of the solitary wave is smaller compared to the prediction of the fKdV equation. Hanazaki (1992) numerically solved the Navier–Stokes equations and got similar results. Melville & Helfrich (1987) proposed the forced extended KdV (fEKdV) equation that has a cubic nonlinear term in addition to the usual quadratic nonlinear term of the fKdV equation. Hanazaki (1992) showed theoretically that the cubic nonlinear term cannot be neglected unless the wave amplitude is extremely small since the coefficient of the quadratic nonlinear term is very small for internal waves in a two-layer fluid.

For axisymmetric inertial waves in swirling flows, Grimshaw (1990) derived the

fKdV equation and Hanazaki (1991, 1993*a*) showed its applicability by comparing its solution with the solution of the Navier–Stokes equations.

For three-dimensional water waves Ertekin (1984) and Ertekin *et al.* (1984) did systematic experiments and found that the upstream solitary waves become straight crested. Later, Cole (1987) solved analytically the linearized equations for three-dimensional water waves and found that the upstream waves become two-dimensional in the long-time limit if the flow is near resonance. To find the applicability of the nonlinear model equations to three-dimensional water waves, Ertekin, Webster & Wehausen (1986) solved the GN equations, Katsis & Akylas (1987) solved the forced Kadomtsev–Petviashvili (fKP) equation and Pedersen (1988), Ertekin & Qian (1990) and Ertekin, Qian & Wehausen (1990) solved the forced Boussinesq equations. They found that, near resonance, the upstream waves become two-dimensional and the amplitude and the generation period of the upstream waves agree with the experiments. From their results, Ertekin (1984), Katsis & Akylas (1987) and Pedersen (1988) argued that the mechanism of the two-dimensionalization is explained by the Mach reflection (Miles 1977*a*, *b*) of the upstream solitary waves at the sidewall of the channel. More recently, Tomasson & Melville (1991) solved an equation similar to the fKP equation that becomes the fKP equation if an additional condition (see their (21)) is assumed. Although their main concern was the internal wave excited by a sidewall perturbation in two-layer flow, the equation can be applied qualitatively well to water waves. When the flow is subcritical, the solution of that equation agreed well with the solution of its linearized version. So they argued that the two-dimensionalization can be explained by the linear theory. They showed that, according to the linear dispersion relation, the lowest mode that spans the entire channel width has the largest group velocity among all the lateral modes. This supports the results by Cole (1987) described above.

For three-dimensional internal waves in a two-layer fluid, Tomasson & Melville (1991) studied the possible effects of the cubic nonlinear term in their model equation as they did for the two-dimensional waves (Melville & Helfrich 1987). They found again similar differences between the solution of the equation with a cubic nonlinear term and that with only a quadratic nonlinear term. Miloh, Tulin & Zilman (1993) showed that the divergence of the solution of the linear theory that occurs at the usual resonance condition can be avoided if the dispersion of the wave is taken into account. Then they solved the linearized equations near resonance, although the generation of upstream waves was not considered. In an experimental study for a supercritical flow, Ma & Tulin (1993) developed a technique that makes possible the accurate measurement of three-dimensional internal waves and compared the downstream wave patterns obtained with the linear theories based on the stationary phase method (Tulin & Miloh 1991). They found a long narrow V-wake behind a ship as in field observations by remote sensing radar, and found good agreement with the linear theories for the wave field sufficiently far from the ship. However, no experimental study exists on three-dimensional nonlinear internal waves. How applicable are the nonlinear theories to three-dimensional stratified flows? Especially, we want to know if the Mach reflection and the subsequent two-dimensionalization of the upstream waves occur as in water waves. We also note here that, even for water waves, the process of Mach reflection of the upstream waves excited by an obstacle has not been thoroughly investigated by experiments or by solving the fully nonlinear equations, although Ertekin (1984) gave a brief sketch of the phenomenon.

The study of internal waves in the flow of a linearly stratified Boussinesq fluid requires special treatment since it is now known that all the nonlinear terms in the KdV-type equations identically vanish in this case. Here, the nonlinearity of the wave

would be quite different from that in the flow of a two-layer fluid (see Appendix to Grimshaw & Yi 1991). Although there are several experimental studies on two-dimensional waves in the flow of a linearly stratified Boussinesq fluid (e.g. Baines 1977, 1979; Castro & Snyder 1988), none of these give a three-dimensional perspective of the upstream wave. Hanazaki (1989*a*) has found that the upstream waves become two-dimensional by solving the three-dimensional Navier–Stokes equations. However, the channel width was too small to investigate the process of the two-dimensionalization of the upstream wave. Theoretically, Grimshaw & Yi (1991) derived a model finite-amplitude equation for the two-dimensional resonant flow and it was quantitatively verified numerically by Hanazaki (1992, 1993*b*). However, the extension of Grimshaw & Yi's theory to three-dimensional waves has yet to be done. Since the linearly stratified Boussinesq fluid is one of the most typical density stratifications that have been extensively studied theoretically and experimentally, the investigation of the three-dimensional aspects of the internal waves in that stratification is also of much interest.

In this study, three-dimensional Navier–Stokes equations for stratified flows are solved numerically. First, near-resonant flow of a nearly two-layer fluid is considered. We show to what extent the waves resonantly excited by an obstacle are describable by the fKP or the fEKP equations. In particular, we show that abnormal reflection similar to Mach reflection occurs at the sidewall and the two-dimensionalization of the upstream waves can be explained by that abnormal reflection. We also check the possibility that the two-dimensionalization is explained by the different group velocities among the lateral modes of the linear wave. Next, subcritical flow of a nearly two-layer fluid is considered. We show that Mach reflection and the subsequent two-dimensionalization of the upstream waves occur again in this case. Finally, results for waves in the flow of a linearly stratified Boussinesq fluid are given. The nonlinearity of the wave would be different in this case and we will see that upstream waves behave differently from waves in the two-layer fluid.

2. Theory

We study the laminar flow of the three-dimensional stratified fluid. Internal waves are generated by topography located on the bottom of a rectangular channel (see figure 1). Upstream flow has a uniform velocity U and a vertical density stratification given by $\bar{\rho}(z)$. The governing equations are the Navier–Stokes equations for an incompressible stratified fluid:

$$\frac{\partial \boldsymbol{v}}{\partial t}+(\boldsymbol{v}\cdot\boldsymbol{\nabla})\,\boldsymbol{v}=-\frac{1}{\rho}\boldsymbol{\nabla}p-g\hat{\boldsymbol{z}}+\frac{\mu}{\rho}\nabla^2\boldsymbol{v}, \tag{2.1a}$$

$$\frac{\partial \rho}{\partial t}+(\boldsymbol{v}\cdot\boldsymbol{\nabla})\,\rho=0, \tag{2.1b}$$

$$\boldsymbol{\nabla}\cdot\boldsymbol{v}=0, \tag{2.1c}$$

where $\boldsymbol{v}=(u,v,w)$ is the velocity, p is the pressure, ρ is the density, μ is the viscosity coefficient, g is the acceleration due to gravity and $\hat{\boldsymbol{z}}$ is the unit vector along the z-axis. Equation (2.1*b*) is the condition of incompressibility and, together with (2.1*c*), assures the conservation of mass.

Although the full Navier–Stokes equations will be solved at a finite Reynolds

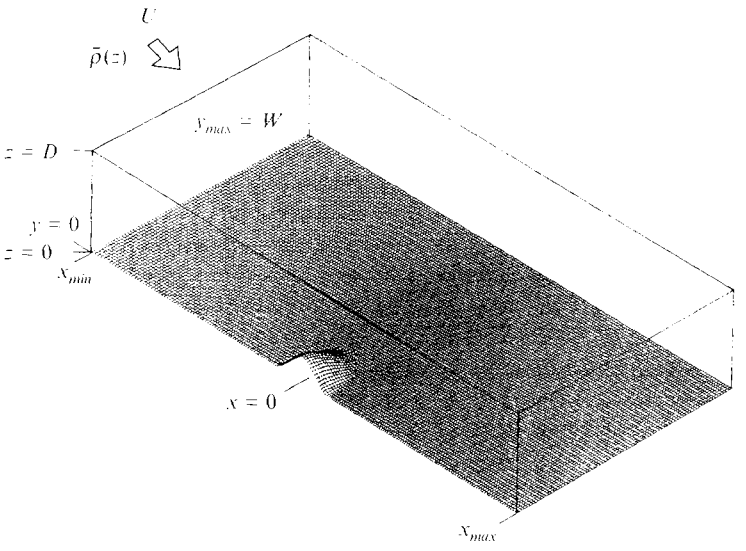

FIGURE 1. Schematic view of the flow geometry.

number in §§3 and 4, we review here briefly the weakly nonlinear theories (the fKP equation and the fEKP equation) derived from the inviscid form of (2.1) for later comparison (§4) with the solution of the Navier–Stokes equations. To derive the fKP equation and the fEKP equation from the inviscid form of (2.1), we rescale x, y and t as

$$X = \epsilon^{\frac{1}{2}}x, \quad Y = \epsilon y, \quad T = \epsilon^{\frac{3}{2}}t, \tag{2.2}$$

where ϵ is a small parameter, and expand dependent variables in powers of ϵ as

$$u = U + \sum_{m=1}^{\infty} \epsilon^m u^{(m)}, \quad v = \sum_{m=1}^{\infty} \epsilon^{m-\frac{1}{2}} v^{(m)}, \quad w = \sum_{m=1}^{\infty} \epsilon^{m+\frac{1}{2}} w^{(m)}, \tag{2.3a–c}$$

$$\rho = \bar{\rho}(z) + \sum_{m=1}^{\infty} \epsilon^m \rho^{(m)}, \quad p = -g\int^z \bar{\rho}(z)\,\mathrm{d}z + \sum_{m=1}^{\infty} \epsilon^m p^{(m)}. \tag{2.3d, e}$$

We scale the obstacle height h as

$$h = \epsilon^2 H(X, Y, T). \tag{2.4}$$

The scalings in (2.2), (2.3) and (2.4) assure the balance between the effects of nonlinearity, dispersion and the forcing by the obstacle in the leading-order terms of the perturbation field.

We assume that the vertical displacement of the fluid ζ is written as

$$\zeta = \epsilon\zeta^{(1)} + O(\epsilon^2) = \epsilon A(X, Y, T)\,\phi_n(z) + O(\epsilon^2). \tag{2.5}$$

Then, at $O(\epsilon)$, we obtain a Sturm–Liouville equation for $\phi_n(z)$:

$$\frac{\mathrm{d}}{\mathrm{d}z}\left(\bar{\rho}C_n^2\frac{\mathrm{d}\phi_n}{\mathrm{d}z}\right) - g\frac{\mathrm{d}\bar{\rho}}{\mathrm{d}z}\phi_n = 0, \tag{2.6a}$$

$$\phi_n(0) = \phi_n(D) = 0, \tag{2.6b}$$

where $C_n (C_1 > C_2 > \ldots)$ and $\phi_n(z)$ are, respectively, the nth eigenvalue and the nth eigenfunction.

We then obtain, at $O(\epsilon^2)$, the fKP equation. If we consider also the effect of the cubic nonlinearity of higher order, i.e. $O(\epsilon^3)$, we obtain the fEKP equation for $A(X, Y, T)$:

$$-\frac{1}{C_n}(A_T + \Delta A_X) + a_1 A A_X + \epsilon a_2 A^2 A_X + a_3 A_{XXX} + \frac{1}{2}\int_{-\infty}^{X} \mathrm{d}X A_{YY} + G_X = 0, \quad (2.7a)$$

where

$$\Delta = \frac{U - C_n}{\epsilon}, \quad (2.7b)$$

$$a_1 = \frac{3\int_0^D \bar{\rho}\left(\frac{\mathrm{d}\phi_n}{\mathrm{d}z}\right)^3 \mathrm{d}z}{2L_n}, \quad a_2 = \frac{3\int_0^D \bar{\rho}\left(\frac{\mathrm{d}\phi_n}{\mathrm{d}z}\right)^4 \mathrm{d}z}{L_n}, \quad a_3 = \frac{\int_0^D \rho\phi_n^2 \,\mathrm{d}z}{2L_n}, \quad (2.7c\text{–}e)$$

$$G(X, Y) = \left(\bar{\rho}\frac{\mathrm{d}\phi}{\mathrm{d}z}\right)_{z=0} \frac{H(X, Y, T)}{2L_n}, \quad L_n = \int_0^D \bar{\rho}\left(\frac{\mathrm{d}\phi_n}{\mathrm{d}z}\right)^2 \mathrm{d}z. \quad (2.7f\text{–}g)$$

The fKP equation is obtained by neglecting the cubic nonlinear term $\epsilon a_2 A^2 A_X$ in (2.7*a*). In a two-dimensional two-layer flow, Melville & Helfrich (1987) found by experiments that the effect of the cubic nonlinearity cannot be neglected and proposed the fEKdV equation. Tomasson & Melville (1991) calculated the ratio of the quadratic and cubic nonlinear terms under the Boussinesq approximation, then solved their model equation for three-dimensional internal waves with a cubic nonlinear term. They found a monotonic-bore solution near resonance (see their figures 11 and 13*b*). Hanazaki (1992) showed that, in a general two-layer fluid, the ratio $\epsilon a_2/a_1$ is very large compared to that in a water wave and the internal waves would be well described by the fKdV equation only when the amplitude of the wave is very small (see his equation (18) and figure 5). In this study the solutions of both the fKP and the fEKP equations are compared with the wave profile $A(X, Y, T)$ obtained from the solutions of the fully nonlinear Navier–Stokes equations.

In the special case of a linearly stratified Boussinesq fluid, (2.6*a*) becomes

$$\frac{\mathrm{d}^2\phi_n}{\mathrm{d}z^2} - \frac{N^2}{C_n^2}\phi_n = 0, \quad (2.8a)$$

where the constant Brunt–Väisälä frequency is given by

$$N^2 = -\frac{g}{\bar{\rho}}\frac{\mathrm{d}\bar{\rho}}{\mathrm{d}z}. \quad (2.8b)$$

Therefore, $\phi_n(z)$ and C_n become

$$\phi_n(z) = \sin(n\pi z/D), \quad (2.9a)$$

and

$$C_n = ND/n\pi. \quad (2.9b)$$

Substituting (2.9*a*) into (2.7*c*, *g*) and setting $\bar{\rho}(z)$ constant in the integrand, we find that $a_1 = 0$, which means that the quadratic nonlinear term in the fKP and fEKP equation vanishes. In this case, the nonlinear correction of the linear wave speed would be very small. This can be expected from the solution of the equation derived by Grimshaw & Yi (1991) and also from the numerical solution of the two-dimensional Navier–Stokes equations (Hanazaki 1992, 1993*b*).

3. Numerical method

The governing equations for the nearly two-layer flow are (2.1*a–c*), while the equations for the linearly stratified Boussinesq fluid are the same as in Hanazaki (1989*a*). The numerical method is an extension of the usual MAC (marker and cell) method for fluid of uniform density to stratified fluid. The body-fitted curvilinear coordinates (Thames *et al.* 1977) are also used. These have been used in previous numerical studies on stratified flows (Hanazaki 1989*a*, *b*, 1992, 1993*b*). The time derivatives are approximated by the forward differences of first-order accuracy. The space derivatives are approximated by central differences of second-order accuracy except for the nonlinear terms where a scheme of third-order accuracy (Kawamura, Takami & Kuwahara 1986) is used.

The computation was done in the domain (see figure 1)

$$x_{min} \leqslant x \leqslant x_{max}, \quad 0 \leqslant y \leqslant y_{max} = W, \quad h(x,y) \leqslant z \leqslant z_{max} = D, \tag{3.1}$$

where W is the half-width of the channel, D is the channel depth and the obstacle shape is given by

$$h(x,y) = h_{max}\frac{1}{2}\left[1+\cos\left(\pi\left\{\left(\frac{x}{5D}\right)^2+\left(\frac{y}{10D}\right)^2\right\}^{\frac{1}{2}}\right)\right] \quad \text{for} \quad \left(\frac{x}{5D}\right)^2+\left(\frac{y}{10D}\right)^2 \leqslant 1 \tag{3.2a}$$

and

$$h(x,y) = 0 \quad \text{for} \quad \left(\frac{x}{5D}\right)^2+\left(\frac{y}{10D}\right)^2 \geqslant 1 \tag{3.2b}$$

with

$$h_{max} = 0.1D. \tag{3.2c}$$

The computation is done only for $y \geqslant 0$ because we assume the symmetry of the flow with respect to the plane $y = 0$. At $y = W$ and $z = D$, rigid walls exist and the waves are reflected by these walls.

The boundary conditions for the nearly two-layer flow are as follows:

on the upstream boundary ($x = x_{min}$),

$$\boldsymbol{v} = (U,0,0) \quad \text{and} \quad \rho = \bar{\rho}(z); \tag{3.3a}$$

and on the downstream boundary ($x = x_{max}$),

$$\frac{\partial \boldsymbol{v}}{\partial t}+u\frac{\partial \boldsymbol{v}}{\partial x} = 0 \quad \text{and} \quad \frac{\partial \rho}{\partial t}+u\frac{\partial \rho}{\partial x} = 0. \tag{3.3b}$$

On the sidewall ($y = y_{max} = W$) and on the lower and the upper boundary

$$(z = h(x,y), z = z_{max} = D),$$

the velocity satisfies the impermeability condition and the free shear stress condition

$$\boldsymbol{v}\cdot\boldsymbol{n} = 0, \quad (\boldsymbol{n}\cdot\nabla)\boldsymbol{v}_t = 0, \tag{3.3c, d}$$

where $\boldsymbol{n}$ is the unit normal to the boundary and $\boldsymbol{v}_t$ is the tangential velocity. The density satisfies

$$\frac{\partial \rho}{\partial y} = 0 \quad \text{on} \quad y = y_{max} = W, \tag{3.3e}$$

$$\rho = \bar{\rho}(0) \quad \text{on} \quad z = h(x,y), \tag{3.3f}$$

and $$\rho = \bar{\rho}(D) \quad \text{on} \quad z = z_{max} = D. \tag{3.3g}$$

In the case of horizontally unbounded flow ($W = \infty$) (see figure 8*b*), the velocity v on the sidewall was determined by a simple extrapolation instead of (3.3*c*, *d*).

The undisturbed density distribution $\bar{\rho}(z)$ is given by

$$\bar{\rho}(z) = \tfrac{1}{2}[\bar{\rho}(0)+\bar{\rho}(D)] - \tfrac{1}{2}[\bar{\rho}(0)-\bar{\rho}(D)]\tanh\left[\frac{50(z-h_2)}{D}\right], \tag{3.4a}$$

with $$\bar{\rho}(D) = 0.9\bar{\rho}(0), \quad h_2 = 0.3D. \tag{3.4b, c}$$

This vertical density distribution is the same as that of the nearly two-layer two-dimensional flow in Hanazaki (1992) and determines the coefficients of the fKP or the fEKP equations from (2.7*c*, *d*, *e* and *g*) (with $n = 1$) as

$$a_1 = 2.99D^{-1}, \quad a_2 = 2.62 \times 10D^{-2}, \quad a_3 = 3.52 \times 10^{-2}D^2, \tag{3.5a–c}$$

when we normalize $\phi_n(z)$ so that $\phi_n(z)_{max} = 1$. For linearly stratified Boussinesq flow also, boundary conditions similar to (3.3) are used.

In this study, the Froude number is defined by

$$F = U/C_1, \tag{3.6}$$

where C_1 is the maximum eigenvalue of the Sturm–Liouville problem (2.6). Specifically, in the case of linearly stratified Boussinesq fluid, C_1 is given by (2.9*b*) (with $n = 1$). The Froude number is varied as $0.6 \leqslant F \leqslant 1.4$. The Reynolds number, defined by

$$Re = \bar{\rho}(0)\, Uh_{max}/\mu, \tag{3.7}$$

is fixed to be 10^3. Here, $\bar{\rho}(0)$ can be used as a representative value of density since the density difference between the top and the bottom of the channel is only 10%. As a representative length, we can also use the channel depth D instead of h_{max}. In this study D and h_{max} are simply related by (3.2*c*).

The value of $Re = 10^3$ was used because recent studies (Hanazaki 1992, 1993*a*, *b*) have shown that, if the Reynolds number is less than about 500, the effect of the viscosity is too strong to investigate the essentially inviscid mechanisms of the generation and propagation of the wave. For comparison with the weakly nonlinear theories that assume inviscid fluid, we need to know what occurs in the limit of infinite Reynolds number. The author has tested the case of $Re = 10^4$ with $F = 1.0$, and found that the upstream wave patterns, including the wave amplitude and the wave generation period, are quantitatively almost unchanged at least until the second upstream wave is generated. Since it sometimes takes a very long time before the effect of the viscosity becomes apparent (e.g. compare figures 1*a* and 8*a* of Smyth 1988), this test might not be sufficient to consider the viscous effects in the long-time limit. However, to know the development of the upstream waves for a sufficiently long time, we can say that the Reynolds number 10^3 is large enough.

We have used grids of $400 \times 80 \times 100$ ($x \times y \times z$) for the channel of $W = 40D$ and $400 \times 40 \times 100$ ($x \times y \times z$) for the channel of $W = 20D$. For both the nearly two-layer flow and the linearly stratified Boussinesq flow, the distribution of the grid points in the z-direction is the same as in Hanazaki (1992) except just above the obstacle, where the differences in the dimensionality and the shape of the obstacle give some differences. For example, in the case of nearly two-layer flow, the grid spacing is small near the interface of the two to capture the rather abrupt density variation. At least seven grid points are distributed across the interface whose thickness is estimated as

$D/50 \times 2$ from (3.4a). The grid is concentrated near the lower boundary [$z = h(x, y)$] to take into account the obstacle shape (3.2) accurately. In the y- direction, the grid spacing is constant ($\Delta y = 0.5D$). In the x-direction, weak stretching which makes the grid a little coarser near the upstream boundary is performed where $x < -5D$. Therefore, Δx is given approximately by $\Delta x = 0.2D$ where $x < -5D$, while it is given exactly by $\Delta x = 0.2D$ where $x > -5D$.

We have tested a grid with $800 \times 40 \times 100$ ($x \times y \times z$) grid points for $W = 40D$. Almost no quantitative differences were found in the upstream waves and the downstream depression region, and therefore, we can say that the grid spacing used in this study is fine enough. For the time differencing, $\Delta(Ut/D) = 0.01$ is used because the use of $\Delta(Ut/D) = 0.005$ showed almost no quantitative differences. Conservation of mass was checked at the inflow and the outflow boundaries. The difference in the total mass that passes through the inflow and the outflow boundaries per unit time was within 0.2% and so we can say that mass conservation is also achieved with high accuracy. Typical CPU time required for the computation up to $Ut/D = 400$ using the $400 \times 80 \times 100$ ($x \times y \times z$) grid was 25 hours on the NEC SX-3 computer (5.5GFLOPS with single processor) of the Centre for Global Environmental Research of the National Institute for Environmental Studies.

To compare the solution of the fully nonlinear Navier–Stokes equations with the weakly nonlinear theory, we also solved the fKP and fEKP equations (2.7)) numerically. The numerical method is the same as in Katsis & Akylas (1987) (see their equation (24)), where an explicit scheme of Lax–Wendroff type was used. The scheme assures third-order accuracy in time and second-order accuracy in space. It does not require the filtering in the y-direction often used to avoid the numerical instability caused by waves of short wavelength. In this study ΔX, ΔY and ΔT were set to be $\Delta(\epsilon^{\frac{1}{2}}X) = 2 \times 10^{-1}D$, $\Delta(\epsilon^{-1}Y) = 5 \times 10^{-1}D$ and $\Delta(\epsilon^{\frac{3}{2}}T) = 5 \times 10^{-6}D/U$. Further reduction of these values (e.g. $\Delta(\epsilon^{\frac{1}{2}}X) = 1 \times 10^{-1}D$ or $\Delta(\epsilon^{\frac{3}{2}}T) = 2.5 \times 10^{-6}D/U$) made almost no quantitative difference to the solution. This assures that the solutions of the fKP and the fEKP equations presented in this paper contain only negligible truncation errors.

4. Results

In figure 2, time development of the resonant ($F = 1.0$) flow of a nearly two-layer fluid over topography is shown. Here $A(x, y, t) = A_1(x, y, t)$ is calculated using the horizontal velocity $u(x, y, z, t)$ that can be written as

$$u(x, y, z, t) - U = -\epsilon C_n \sum_{n=1}^{\infty} A_n(x, y, t) \frac{\mathrm{d}\phi_n}{\mathrm{d}z} + O(\epsilon^2). \tag{4.1a}$$

By using the orthogonality condition of the eigenfunctions:

$$\delta_{mn} I_n = C_n^2 \int_0^D \bar{\rho}(z) \frac{\mathrm{d}\phi_m}{\mathrm{d}z} \frac{\mathrm{d}\phi_n}{\mathrm{d}z} \mathrm{d}z, \tag{4.1b}$$

$A_n(x, y, t)$ is calculated as

$$A_n(x, y, t) \approx -\frac{C_n}{\epsilon I_n} \int_0^D (u(x, y, z, t) - U) \bar{\rho}(z) \frac{\mathrm{d}\phi_n}{\mathrm{d}z} \mathrm{d}z. \tag{4.1c}$$

We should note that the value of $A_n(x, y, t)$ thus obtained contains an error of $O(\epsilon)$.

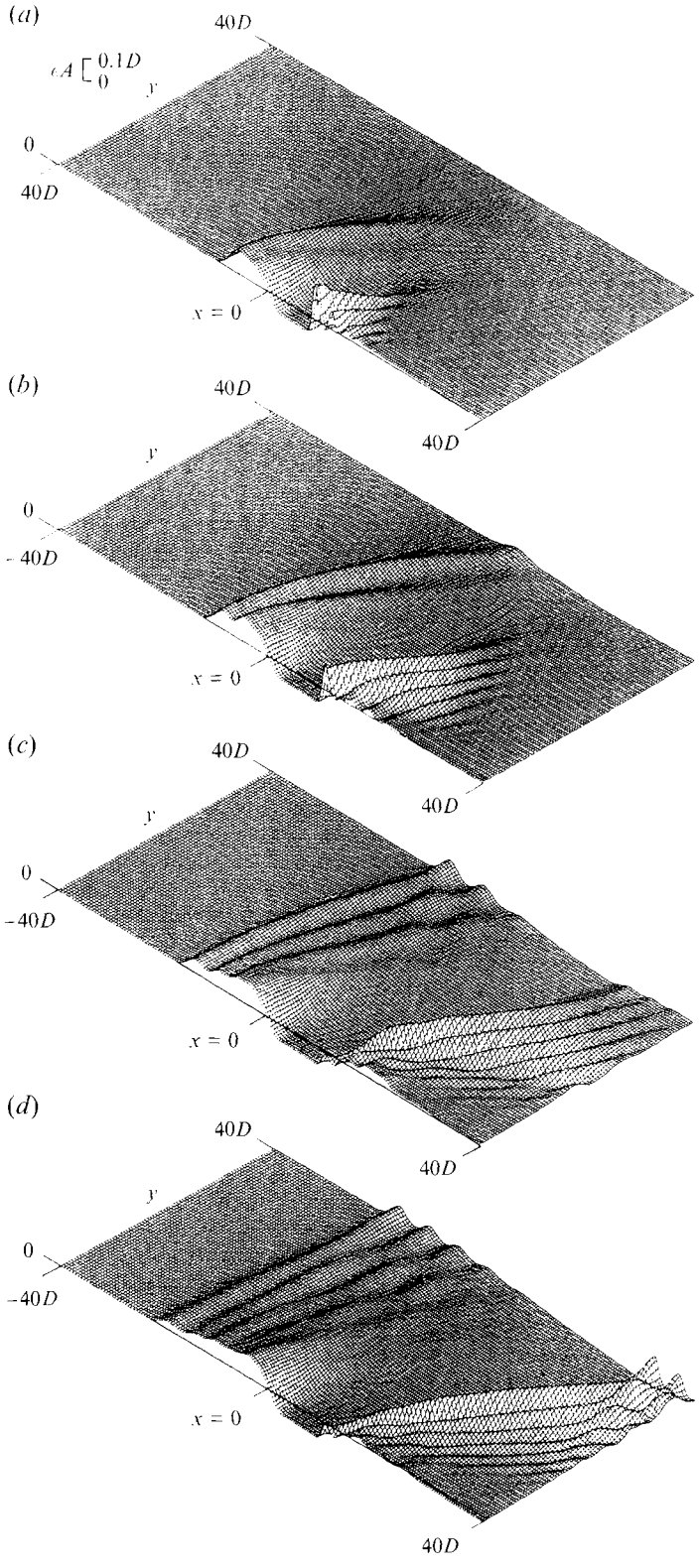

FIGURE 2. Time development of $A(x, y, t)$ obtained from the solution of the Navier–Stokes equations when $F = 1.0$ (two-layer flow): (*a*) $Ut/D = 40$; (*b*) $Ut/D = 80$; (*c*) $Ut/D = 200$; (*d*) $Ut/D = 400$.

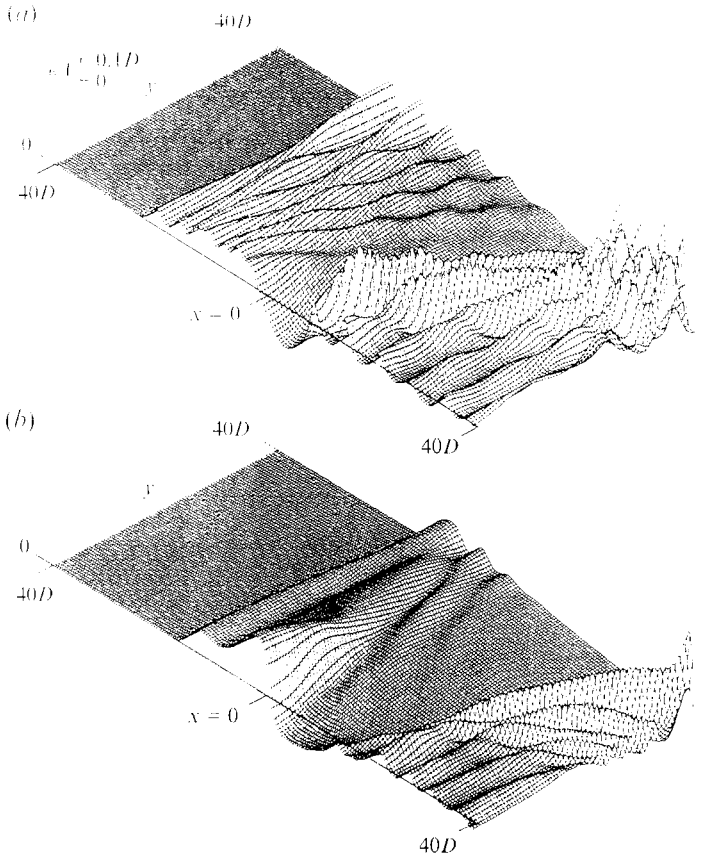

FIGURE 3. $A(x, y, t)$ obtained from the solution of the weakly nonlinear equations when $F = 1.0$ (two-layer flow, $Ut/D = 200$): (*a*) fKP equation; (*b*) fEKP equation.

In the initial period ($Ut/D = 40$), the upstream waves are curved backwards (figure 2*a*). At around $Ut/D = 60$, the far side ends of the upstream waves reach the sidewall and begin to be reflected. After that, the upstream waves become gradually straight crested as time proceeds because the propagation speed of the upstream wave is faster near the sidewall ($y = 40D$) than near the centreplane ($y = 0$). This difference in the propagation speed is because the wave amplitude is larger near the sidewall than near the centreplane. This occurs because the waves are reflected at the sidewall and waves perpendicular to the wall appear (see also Figure 5). Downstream of the obstacle, a flat depression is formed and it becomes longer as time proceeds. Although its length becomes nearly invariant after $Ut/D = 200$ just downstream of the obstacle ($x > 0, y \approx 0$), it is still elongated near the sidewall until at least $Ut/D = 400$. Further downstream, lee waves are generated which also propagate obliquely to the sidewall and finally begin to be reflected (figure 2*d*).

To compare this solution to the weakly nonlinear theory, the solutions of the fKP and fEKP equations (see (2.7)) when $F = 1.0$ ($Ut/D = 200$), with a_1, a_2 and a_3 given by (3.5), are shown in figure 3. The overall qualitative features agree with the solution of the fully nonlinear Navier Stokes equations. That is, upstream advancing waves, downstream depressions and lee waves appear in these solutions. However, there are some quantitative differences. A nearly flat depression just downstream of the obstacle

($x > 0, 1' \approx 0$), which is typical in two-dimensional waves and also seen in the three-dimensional solution of the Navier–Stokes equations. does not appear in the solutions of the fKP and fEKP equations, although in the solution of the fEKP equation. the curve of the depression is weaker. In addition, in the solution of the fKP equation (figure 3*a*), the generation period of the upstream waves is shorter and the upstream-advancing speed is larger. These differences are the same as for the two-dimensional fluid (Melville & Helfrich 1987; Hanazaki 1992). Although the upstream waves have comparable amplitudes, the lee-wave amplitude is highly over-predicted. In the solution of the fEKP equation (figure 3 *b*), the amplitude of the upstream wave is over-predicted although the lee-wave amplitude is smaller than that from the solution of the fKP equation. The generation period of the upstream wave is longer and the upstream-advancing speed is smaller than from the solution of the Navier-Stokes equations. It seems that, except just upstream of the obstacle ($x \leqslant 0, y \leqslant 20D$), the fEKP equation shows better agreement with the Navier-Stokes equations than the fKP equation. However, the solution of the fEKP equation shows large differences just upstream of the obstacle ($x \leqslant 0, y \leqslant 200$) where we have most concern. Therefore, we cannot say without qualification that the fEKP equation is a sufficiently accurate model of the phenomenon. We note that, although comparisons are made here only for $F = 1.0$, typical qualitative differences were the same for the other Froude numbers near resonance. In the solution of the fEKP equation, the monotonic bore shown in Tomasson & Melville (1991) (see their figure 13 *b*) did not appear. This may be because the amplitude of the upstream wave was smaller in this study than in theirs.

It should be noted that in figures 2 and 3 the amplitude of the upstream wave becomes smaller as it propagates. Previous solution of the weakly nonlinear equations (Ertekin *et* al. 1986, figure 1 ; Katsis & Akylas 1987, figure 3(n); and Tomasson & Melville 1991, figure 6(h)) all show that upstream waves have equal amplitude that is invariant with time. However, this would occur only after a much longer time has passed and the upstream waves have become nearly completely straight crested or two-dimensional. In this study, even in the last stage of the time evolution, the upstream waves develop still three-dimensionally. This is because the channel is wide so that the time required for the two-dimensionalization of the upstream wave is long compared to the wave-generation period. Therefore, the waves develop in a similar way to the waves in a horizontally unbounded fluid. In fact, in the solution of the fKP equation for horizontally unbounded fluid, Lee & Grimshaw (1990) found that the upstream waves have larger amplitude near the obstacle (see their figures 1, 4, 5 and 6). In the solution of the forced Boussinesq equations, Pedersen (1988, figure 9) showed the same result. He also found that the height variation in the x-direction is reversed on moving toward the open boundary from the centreplane, and near the open boundary the foremost wave has the largest amplitude (see his figure 9). This also agrees with our figures 2 and 3. If we use an obstacle of smaller height, the wave-generation period would become longer, or if we use a narrower channel, reflection of the wave at the sidewall occurs faster and two-dimensionalization occurs faster. In those cases the wave-generation period would become comparable with the time required for the two-dimensionalization of the upstream wave and upstream waves of equal amplitude would be generated (see also figure 8*a*).

To see the Froude-number dependence of the wave, results for various Froude numbers at $Ut/D = 200$ are shown in figure 4. When $F = 0.9$, upstream waves are weak compared to when case of $F = 1$ .O (figure 2 *c*). The upstream-advancing speed is faster because of the faster linear-wave speed and the wave-generation period is shorter. The length of the downstream depression is smaller and the lee-wave amplitude is larger.

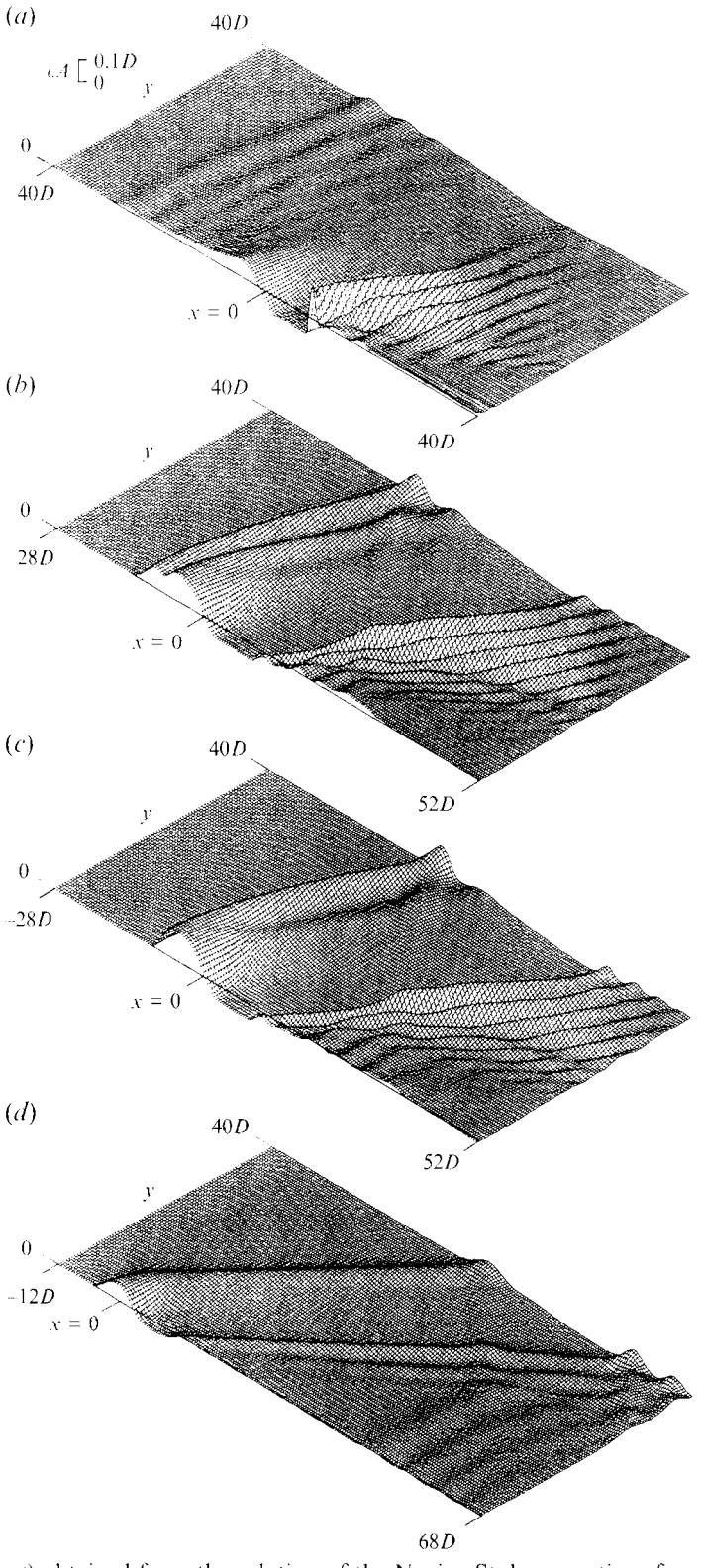

FIGURE 4. $A(x, y, t)$ obtained from the solution of the Navier–Stokes equations for various Froude numbers (two-layer flow, $Ut/D = 200$): (*a*) $F = 0.9$; (*b*) $F = 1.05$; (*c*) $F = 1.1$; (*d*) $F = 1.4$.

These differences, especially near the centreplane ($y = 0$), are essentially the same as in two-dimensional flows. When $F = 1.05$, the upstream waves have larger amplitude and longer wave-generation period. Even when $F \geqslant 1$, upstream waves generation has a long-time development as has been predicted by the weakly nonlinear theories. When $F = 1.1$, the upstream waves have even larger amplitude but have an even longer wave-generation period. When $F = 1.4$ and the flow is supercritical, the upstream waves are no longer generated and an elevation of fluid just above the topography is trailing obliquely downstream, having an angle about $\theta = 45°$ to the primary flow direction. This angle approximately agrees with the value determined by $U\cos\theta = C_1$, or equivalently, by $\theta = \cos^{-1}(1/F) = \cos^{-1}(1/1.4) = 41°$. The downstream depression is also formed at this Froude number although it is not flat near $y = 0$. For supercritical flows, Ma & Tulin (1993) found a V-wake behind a ship model. Their results are for larger Froude number ($F \geqslant 3$), but our downstream wave patterns for $F = 1.4$ also show a similar V-wake, which will become narrower for larger Froude numbers.

A controversial issue raised here is the mechanism of the two-dimensionalization of the upstream wave. By solving the fKP or the forced Boussinesq equations, Katsis & Akylas (1987) and Pedersen (1988) explained this two-dimensionalization in the water-wave problem by Mach reflection of the Boussinesq solitary wave at the sidewall. Mach reflection of a Boussinesq solitary wave of sech^2 profile was theoretically considered by Miles (1977*a*, *b*, 1979). Later Melville (1980) showed that, in the theory of Miles (1977*a*, *b*), the mass and the energy are conserved while the momentum is not and this causes the discrepancy between the theory and his experiments. Funakoshi (1981) showed, by solving the equations for water waves which retain only the terms of the lowest-order nonlinearity, that Miles' theory is correct if the wave amplitude is small and the sech^2 profile of the Boussinesq solitary wave is retained. Therefore, although the theory is not yet fully confirmed quantitatively, it is known that some abnormal reflection occurs when a solitary wave is incident on a wall at a small angle. On the other hand, Tomasson & Melville (1991) showed that the phenomenon can be interpreted as the separation of the lateral modes due to the differences in the group velocity of the linear wave.

To see the two-dimensionalization more clear, contours of $A(x, y, t)$ corresponding to figure 2 are shown in figure 5. At first ($Ut/D = 40$, figure 5*a*), the upstream wave is curved backwards as seen also in figure 2, but after the side end of the wave reaches the sidewall at about $Ut/D = 60$, the wave is reflected and a third wave whose wave crest is perpendicular to the sidewall appears (figure 5*b*). This third wave is similar to the Mach stem which appears in Mach reflection. This third wave becomes longer as time proceeds, forming a straight-crested wave front. The upstream-advancing speed of the Mach-stem like wave is faster than the wave near the centreplane because the amplitude is larger. In addition, the stem becomes longer roughly proportional to time. Therefore, the upstream front becomes two-dimensional as time proceeds. The amplitude of the reflected wave is very weak compared with the incident wave, although in figure 5(*c*–*d*) the second upstream wave overlaps the reflected wave and it becomes difficult to know the amplitude of the reflected wave. Also, the angle of reflection is larger than the incident angle in figure 5(*b*–*d*) (see also table 1). These features all agree with the Mach reflection mechanism.

In figure 6, contours of $A(x, y, t)$ for various Froude numbers a short time after the foremost upstream wave begins to be reflected are shown. When upstream-advancing waves are generated ($F = 1.0$, 1.05 and 1.1) (see figures 5*b*, 6*a*, *b*), the reflection angle is larger than the incident angle and the reflection pattern is qualitatively the same for all the Froude numbers near resonance ($F \approx 1$). Although it is difficult to exactly

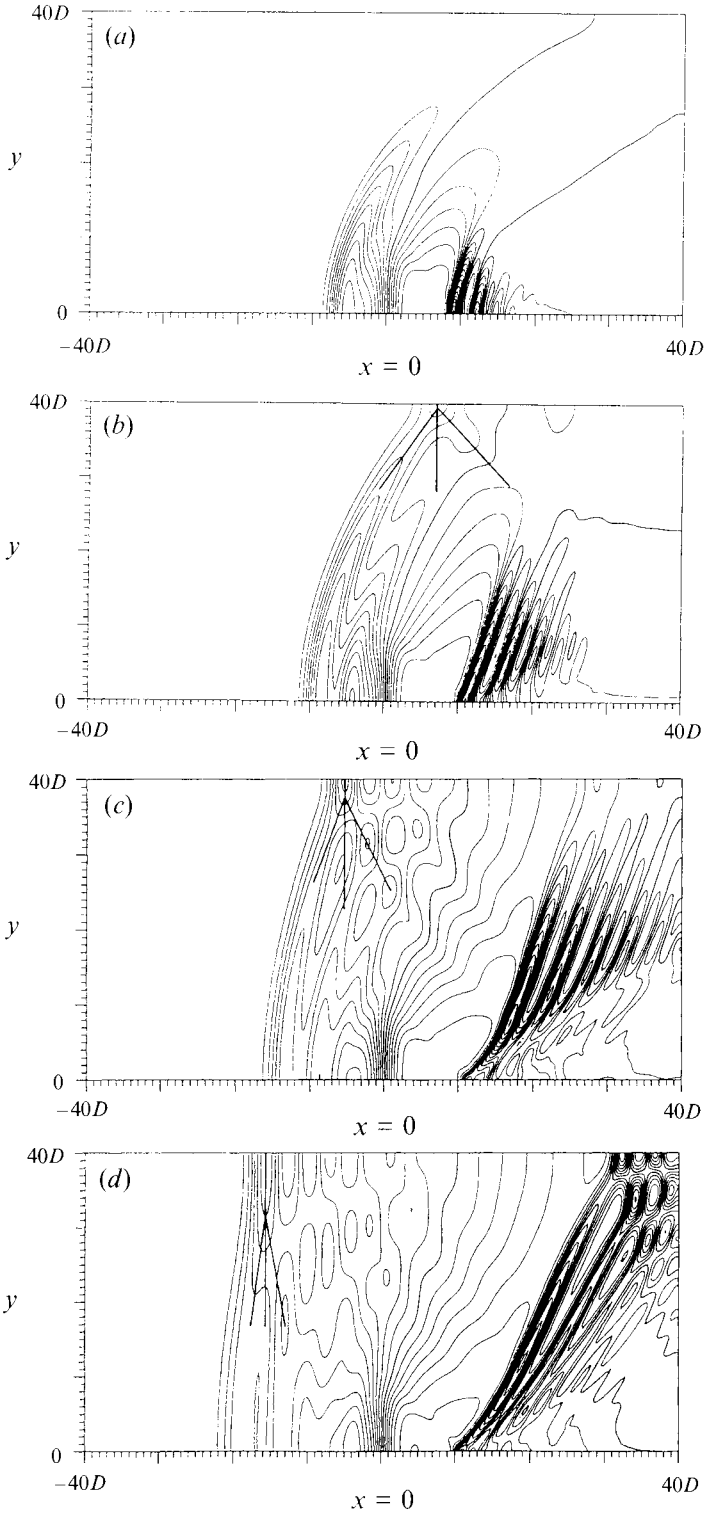

FIGURE 5. Time development of contours of $A(x, y, t)$ obtained from the solution of the Navier–Stokes equations when $F = 1.0$ (two-layer flow): (*a*) $Ut/D = 40$; (*b*) $Ut/D = 80$; (*c*) $Ut/D = 200$; (*d*) $Ut/D = 400$. In (*b*), (*c*) and (*d*), the Mach stem perpendicular to the sidewall and the directions of the incident and reflected waves are shown by additional straight lines.

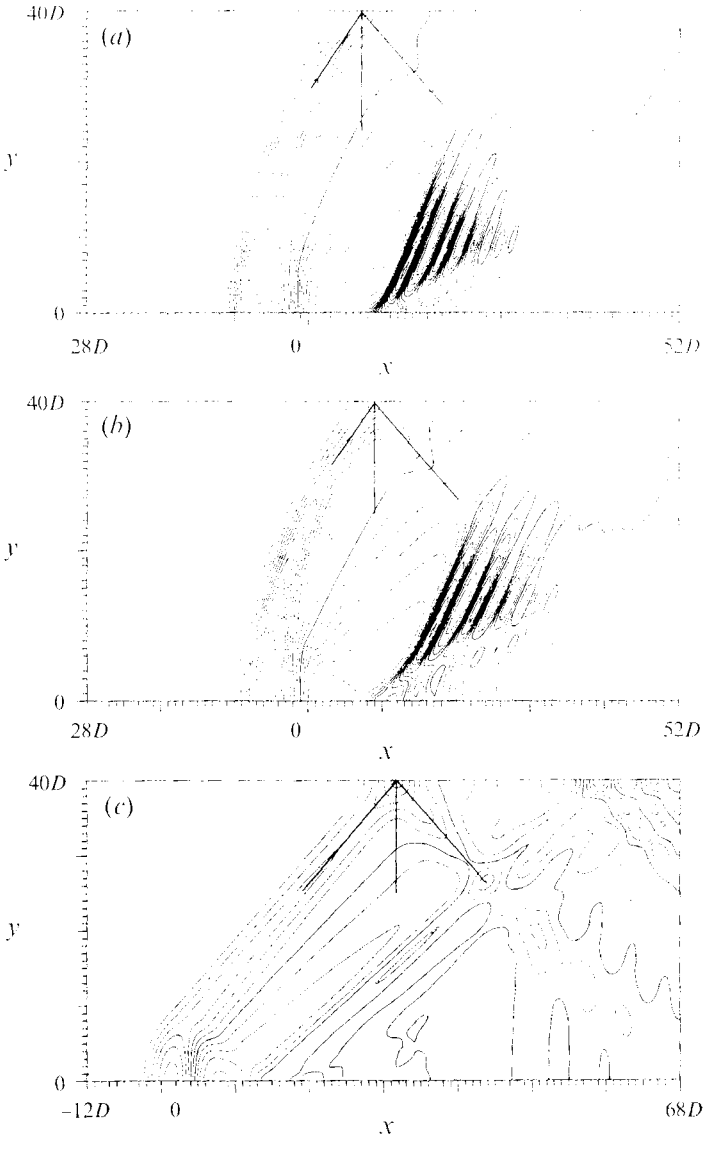

FIGURE 6. Contours of $A(x, y, t)$ obtained from the solution of the Navier-Stokes equations for various Froude numbers (two-layer flow). (*a*) $F = 1.05$ ($Ut/D = 100$); (*b*) $F = 1.1$ ($Ut/D = 120$); (*c*) $F = 1.4$ ($Ut/D = 200$). The interval of the contour is $\Delta(\epsilon A) = 0.01D$. The Mach stem perpendicular to the sidewall and the directions of the incident and reflected waves are shown by additional straight lines.

determine the incident and reflection angles because both the incident and reflected waves are curved and there are some ambiguities in determining these angles, the reflection angle is consistently more than 6° larger than the incident angle as shown table 1. As is typical in Mach reflection, the amplitude of the reflected wave is weaker than the incident wave, although the reflection process is unsteady and the amplitude of the reflected wave is still growing in these figures. These features qualitatively show that the reflection process near the resonant Froude number cannot be explained by normal reflection, and agrees with the Mach reflection discussed by Miles (1977*a*, *b*).

Froude number	Time (Ut/D)	Channel width (D)	Incident angle (deg.)	Reflection angle (deg.)	Difference (deg.)
0.6	70	20	11	18	7
0.9	80	40	29	36	7
1.0	80	40	35	43	8
1.05	100	40	35	42	7
1.1	120	40	35	41	6
1.4	200	40	41	41	0

TABLE 1. Incident and reflection angles of the upstream waves at the sidewall for various Froude numbers

It should be noted that Miles' theory is intended for a Boussinesq solitary wave of sech^2 profile. In this study, the upstream wave pattern does not agree quantitatively with the solution of the fKP equation and may not have the exact sech^2 profile. However, the upstream wave pattern is similar to the Boussinesq solitary wave and shows a qualitatively similar reflection pattern.

When the flow is supercritical and no upstream waves are generated ($F = 1.4$, figure 6*c*), the incident angle and the reflection angle agree (41°) (see table 1) and the amplitude of the reflected wave is comparable with the incident wave. This means that the reflection is a normal reflection. Note that the wave patterns are quite similar to the solution of the forced Boussinesq equations for water waves at the same Froude number (figure 1*a*, *b* of Pedersen 1988).

From table 1, we see that the critical incident angle, which is determined as the boundary between the normal and Mach reflection, is approximately 40° in this study. This value seems to be large compared to the prediction of the theory by Miles (1977*b*) (see table 4 of Pedersen 1988). In an experiment, Perroud (1957) showed that the critical angle is 45° independent of the amplitude of the incident wave when the amplitude is fairly large. In this study also, the amplitude of the upstream wave is large in the sense that the upstream wave profile does not agree with the fKP equation. Therefore, the critical angle would become large. Recently, Tanaka (1993) solved the 'almost' fully nonlinear equations for three-dimensional water waves. He found that, when the wave amplitude divided by the water depth is 0.3, the critical angle is 37.8°. This value is also consistent with our results.

To see if the two-dimensionalization is a result of the linear dispersion relation, we consider the dispersion relation of the unforced linearized KP equation as done by Tomasson & Melville (1991). If we substitute

$$A(X, Y, T) \propto \mathrm{e}^{\mathrm{i}(kx-\omega t)} \cos(l\pi y/W), \tag{4.2}$$

into the linearized KP equation without a forcing term (cf. (2.7)) noting that x, y and t are scaled as in (2.2), we obtain the dispersion relation

$$\omega = C_n\left(a_3 k^3 - \frac{l^2\pi^2}{2W^2 k}\right) + \epsilon\Delta k, \tag{4.3}$$

and the corresponding group velocity

$$C_g = \frac{\partial\omega}{\partial k} = C_n\left(a_3 3k^2 + \frac{l^2\pi^2}{2W^2 k^2}\right) + \epsilon\Delta. \tag{4.4}$$

We note here that the form of the dispersion relation (4.3) is different from (2.7) of

Tomasson & Melville (1991) because they used a slightly different set of equations (see their (2.1*a*, *b*)) from the fKP equation. If we assume an additional relation (see their (2.11)), their equations (2.1*a*, *b*) agree with the fKP equation and the dispersion relation becomes (4.3). In other words, Tomasson & Melville (1991) did not solve the usual fKP equation so that the dispersion relation (see their (2.7) and figure 1) and hence the behaviour of the wave would be somewhat different from ours, although we note that our (4.3) and (2.7) of Tomasson & Melville (1991) agree in that the lowest mode can have the maximum upstream-advancing group velocity and as l increases, the speed becomes slower.

We know from (4.4) that the maximum group velocity

$$C_{g\,max} = C_n(6a_3)^{\frac{1}{2}}\frac{l\pi}{W} + \epsilon\Delta \tag{4.5a}$$

occurs at

$$k = (l^2\pi^2/6a_3W^2)^{\frac{1}{3}}. \tag{4.5b}$$

Therefore, the difference in the speed of the foremost wave of lateral modes $l = 0$ and $l = 1$ (with $n = 1$) is obtained as

$$(6a_3)^{\frac{1}{2}}\frac{l\pi}{W}\frac{U}{F}. \tag{4.6}$$

To see if this result of the linear dispersion relation can be applied to the solution of the Navier–Stokes equations, the time development of the lateral wave modes $l = 0$ and $l = 1$ when $F = 1.0$ is shown in figure 7. Because $A(x, y, t)$ can be decomposed by complete orthogonal functions as

$$A(x, y, t) = \sum_{l=0}^{\infty} \tilde{A}_l(x, t)\cos(l\pi y/W), \tag{4.7a}$$

the amplitude of the each lateral wave mode is calculated by

$$\tilde{A}_l(x, t) = \frac{2}{W}\int_0^W A(x, y, t)\cos(l\pi y/W)\,\mathrm{d}y. \tag{4.7b}$$

At $Ut/D = 200$, the distance between the position of the foremost upstream wave of modes $l = 0$ and $l = 1$, estimate by (4.6) ($F = 1.0, W = 40D$) using (3.5*c*), is $7.2D$. However, we see in figure 7 that the propagation speed of the upstream front is almost the same for modes $l = 0$ and $l = 1$. In the initial time development, not only the lowest mode $l = 0$ but also higher modes ($l \geqslant 1$) are excited and propagate upstream at an almost equal speed. Therefore, the upstream wave is not governed by the linear dispersion relation, at least near resonance. Although Tomasson & Melville (1991) showed the separation of transverse modes when $F = 0.6$ which may be the result of the linear dispersion relation, they did not report such a separation when the flow is near resonance ($F = 1.05$). They argued that only the lowest mode ($l = 0$) can be resonant and develop nonlinearly to form two-dimensional upstream waves. However, the present solution of the Navier–Stokes equations shows that the higher modes ($l \geqslant 1$) also develop nonlinearly and propagate upstream.

The decrease in the amplitude of the mode $l = 1$ with time can be interpreted as follows. When reflection at the sidewall occurs, the value of $A(x, y, t)$ becomes larger with time near the sidewall ($y \geqslant \frac{1}{2}W$) where $\cos(\pi y/W)$ is negative. This works to reduce the value of $\tilde{A}_1(x, t)$. Although the results are not shown here, $\tilde{A}_2(x, t)$ reduces

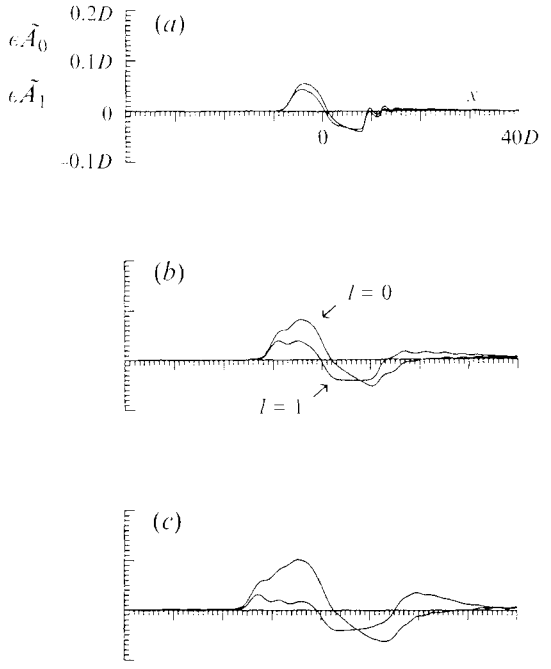

FIGURE 7. Time development of the lateral modes $\tilde{A}_0(x,t)$ and $\tilde{A}_1(x,t)$ in the solution of the Navier–Stokes equations when $F = 1.0$ (two-layer flow): (*a*) $Ut/D = 40$; (*b*) $Ut/D = 100$; (*c*) $Ut/D = 200$.

similarity. The reduction of the wave-front amplitude of modes $l = 1$ and $l = 2$ corresponds to the dominance of mode $l = 0$ and the resultant two-dimensionalization of the upstream wave. We note here that the qualitative feature of the time development of $\tilde{A}_l(x,t)$ ($l = 0$, 1, and 2) was the same for the other near-resonant Froude numbers ($F = 0.9$, 1.05, 1.1).

In figure 8, the effect of the channel width on the upstream wave is shown. When the channel width is small ($W = 20D$), the two-dimensionalization of the upstream wave occurs faster because the reflection of the upstream wave begins sooner. Therefore, the foremost wave is already approximately two-dimensional at $Ut/D = 200$. In this case, the time required for the two-dimensionalization of the upstream wave is smaller and is comparable with the wave generation period. Therefore, nearly straight-crested upstream waves appear to be generated as we noted earlier in the discussions of figure 2 and 3. When the channel width is infinite (or when there is no sidewall), reflection does not occur and two-dimensionalization does not occur. By comparing these figures with figure 4(*b*), we note that until $Ut/D = 200$, the wave-generation period is nearly independent of the channel width. Previous studies on water waves (e.g. Ertekin 1984; Ertekin & Qian 1989) show that, as the blockage coefficient increases, the wave-generation period decreases. The difference probably comes from the fact that the ratio of the channel width to the wavelength of the upstream solitary wave is much larger in this study. For example, in the study of Ertekin (1984), the ratio is generally about less than 2, if we estimate it from his figure 131 ($F = 1.0$), where the widest channel is used in his experiments. In most of his experiments, the upstream wave becomes nearly straight crested before the first solition has been detached. In this study, the ratio is about 4 even for the narrowest channel ($W = 20D$). Therefore, the channel width is effectively larger and it takes a longer time for the upstream waves to become two-

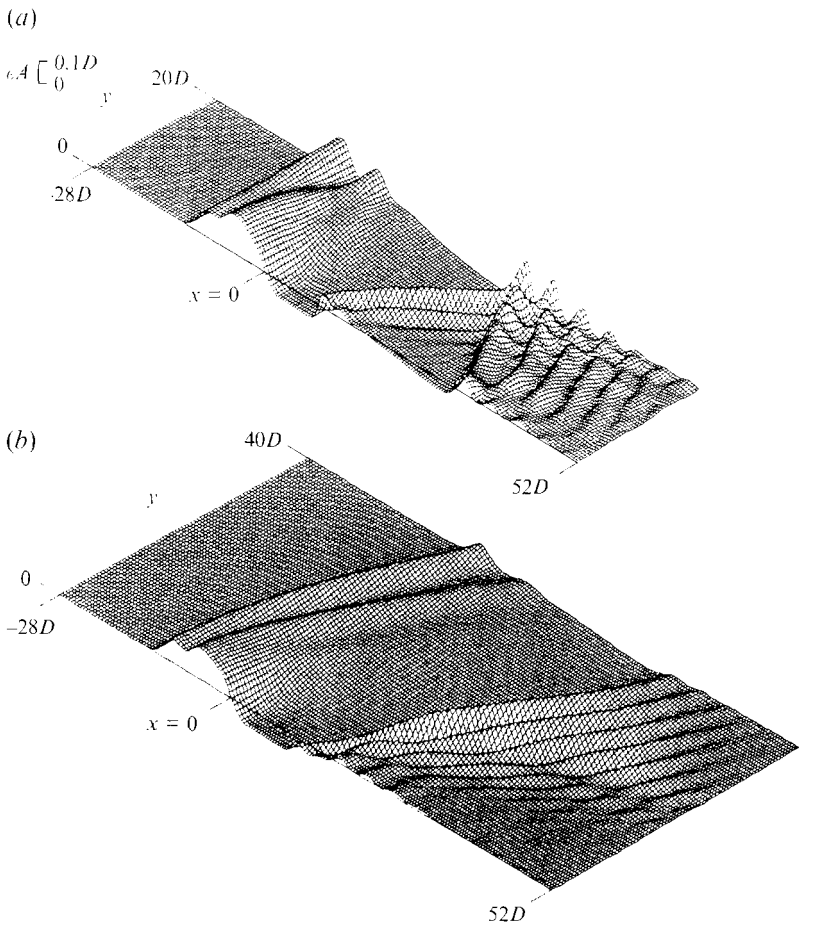

FIGURE 8. Effect of the channel width when $F = 1.05$ (two-layer flow, $Ut/D = 200$): (*a*) $W = 20D$; (*b*) $W = \infty$.

dimensional. Lee & Grimshaw (1990) (see their C_2 in (13)) showed that in the solitary-wave solution of the unforced KP equation, the energy flux velocity in the y-direction is proportional to λ_x/λ_y, where λ_x and λ_y are respectively the wavelength in the x- and y-directions. This qualitatively supports our conjecture since for wider channels, waves of larger λ_y will become dominant. The blockage coefficient would determine the period of the upstream-wave generation after sidewall effect becomes prevailing and the upstream waves become two-dimensional. However, until the far side end of the wave reaches the sidewall, the waves would develop freely as if they were in a horizontally unbounded fluid. In this study, at least one upstream wave has been detached from the obstacle before the sidewall effect becomes very apparent. Therefore, the wave-generation period in this study was almost independent of the channel width. However, if we investigate a much longer time span, the period may become a function of the channel width. The amplitude of the upstream wave is somewhat larger for $W = 20D$ and this would result in a smaller wave-generation period in the longer time span.

To see if the two-dimensionalization of the upstream wave occurs at subcritical Froude numbers, the results for $F = 0.6$ are shown in figures 9 and 10. After the

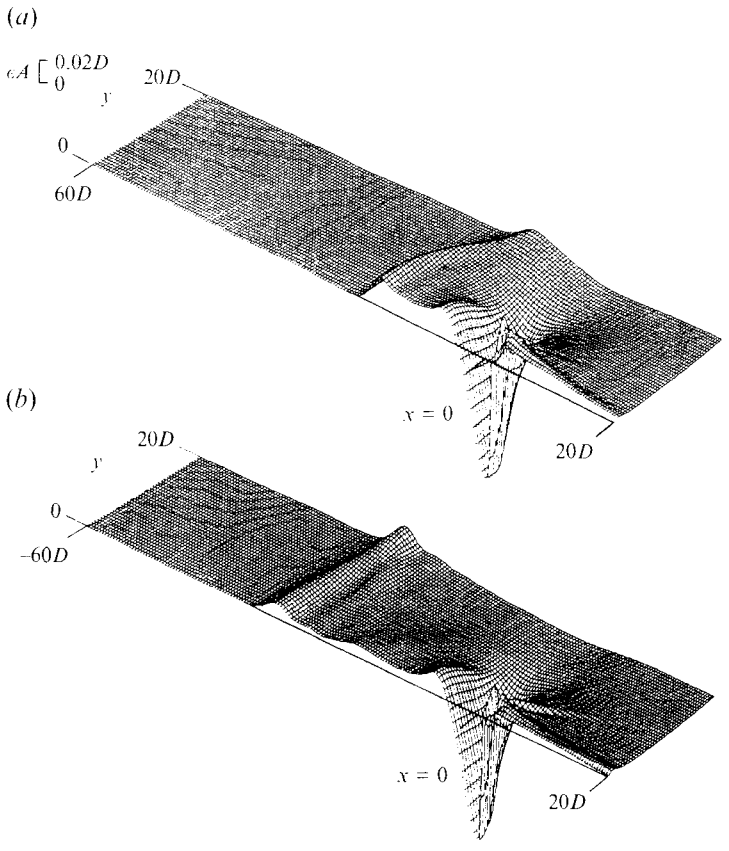

FIGURE 9. Time development of $A(x, y, t)$ obtained from the solution of the Navier–Stokes equations when $F = 0.6$ (two-layer flow): (*a*) $Ut/D = 30$; (*b*) $Ut/D = 70$.

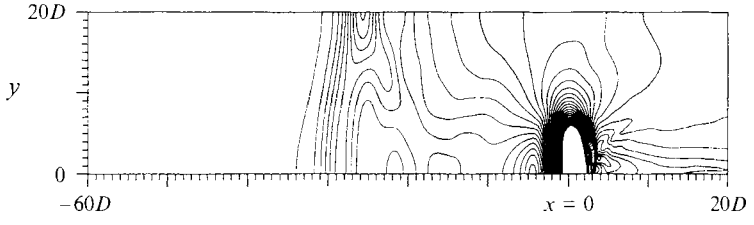

FIGURE 10. Contours of $A(x, y, t)$ obtained from the solution of the Navier–Stokes equations when $F = 0.6$ (two-layer flow, $Ut/D = 70$). The interval of the contour is $\Delta(\varepsilon A) = 0.002D$.

reflection at the sidewall occurs, the upstream wave becomes straight crested as time proceeds. Figure 9 and 10 show reflection patterns similar to the case of the near-resonant flow (figures 2, 5*b* and 6*a*, *b*). Here again, the reflection angle is larger than the incident angle (see table 1) and the amplitude of the reflected wave is much smaller than the incident wave. These patterns are different from the solution of the weakly nonlinear equation given by Tomasson & Melville (1991) at the same Froude number. They showed clear separation of modes $l = 0$, 1 and 2 in their figures 1, 2 and 3, each mode having sinusoidal structure in the x-direction. In addition, the upstream wave pattern was very similar to the solution of the linearized equations. From those figures, they argued that the two-dimensionalization occurs because of the difference in the

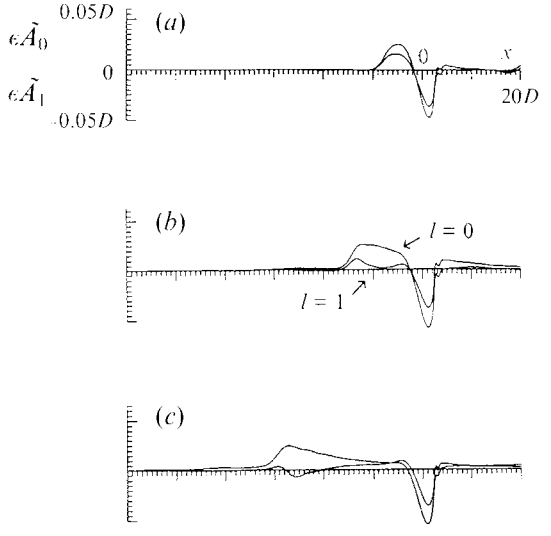

FIGURE 11. Time development of the lateral modes $\tilde{A}_0(x,t)$ and $\tilde{A}_1(x,t)$ in the solution of the Navier–Stokes equations when $F = 0.6$ (two-layer flow): (*a*) $Ut/D = 10$; (*b*) $Ut/D = 30$; (*c*) $Ut/D = 70$.

propagation speed of the lateral modes of the linear wave. The difference occurs partly because the governing equations and the corresponding dispersion relation are slightly different from the present case and the upstream waves behave differently, as noted earlier. However, we note that the two-dimensionalization occurs in figures 9 and 10 even when such 'separation' does not occur.

To see this, the time development of each lateral mode is shown in figure 11. At time $Ut/D = 70$, the difference in the position of the foremost waves of modes $l = 0$ and $l = 1$, estimated by (4.6) ($F = 0.6$, $W = 20D$) using (3.5*c*), is $8.4D$. The upstream waves from the solution of the Navier–Stokes equations do not have a sinusoidal structure and the dispersion relation (4.3) cannot be applied directly to estimate the wave propagation speed quantitatively. However, we see again that each wave mode has almost the same propagation speed. We see only the reflection pattern similar to Mach reflection as in the near-resonant flows. Even when the flow is subcritical, the upstream waves develop nonlinearly. This is because the generated upstream wave has a profile similar to the Boussinesq solitary wave rather than a sinusoidal wave. Therefore, abnormal reflection similar to Mach reflection occurs. The generation of solitary waves at subcritical Froude numbers agrees with the experiments for three-dimensional water waves by Ertekin (1984). He found that solitary waves of elevation are found for Froude numbers as low as 0.2.

It seems that only one upstream wave is generated when $F = 0.6$. The wave pattern near the centreplane ($y = 0$) at $Ut/D = 70$ (figure 9*b*) shows 'two' upstream waves but the second wave appears because the wave reflected at the sidewall returns again to the centreplane. This result is similar to two-dimensional subcritical flow and the corresponding solution of the fKdV equation (see figures 8*b* and 9 of Grimshaw & Smyth 1986) where only a finite number of upstream solitary waves is generated.

Finally we consider the case of linearly stratified Boussinesq flow. Here, the word 'Boussinesq' means that the governing equations assume the Boussinesq approximation. In this case the resonant wave may be governed by the three-dimensional version of the equation derived by Grimshaw & Yi (1991) although it has yet to be

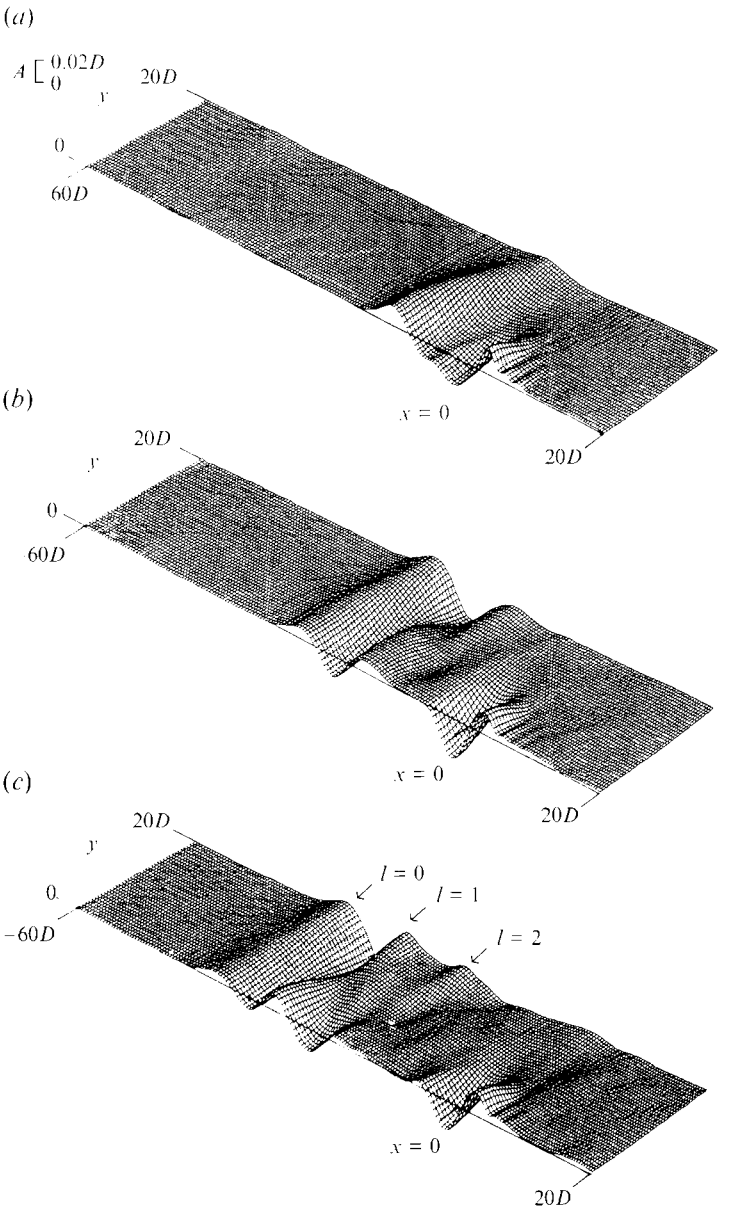

FIGURE 12. Time development of $A(x, y, t)$ obtained from the solution of the Navier–Stokes equations when $F = 0.6$ (linearly stratified Boussinesq flow): (*a*) $Ut/D = 20$; (*b*) $Ut/D = 50$; (*c*) $Ut/D = 80$.

derived. Because the two-dimensionalization of the upstream wave has also been shown in the subcritical flow of linearly stratified Boussinesq fluid (Hanazaki 1989*a*, figure 8), it is of interest to see what occurs in detail in these flows. As an example, we show the case of $F = 0.6$ in figures 12 and 13. In figure 12, $A(x, y, t)$ is calculated using (4.1) with ϕ_n and $C_n (n = 1)$ given by (2.9*a*, *b*). Here, $\epsilon = 1$ is used in (4.1) because in two-dimensional flow, it is found that forcing of $O(\epsilon)$ excites a wave of $O(1)$ (Grimshaw & Yi 1991; Hanazaki 1992, 1993*b*). In linearly stratified Boussinesq flow, a parameter K defined by $K = ND/\pi U = 1/F$ has often been used. It should be noted that $F = 0.6$ corresponds to $K = \frac{5}{3}$. We see a clear separation of the modes $l = 0$ and $l = 1$ in this

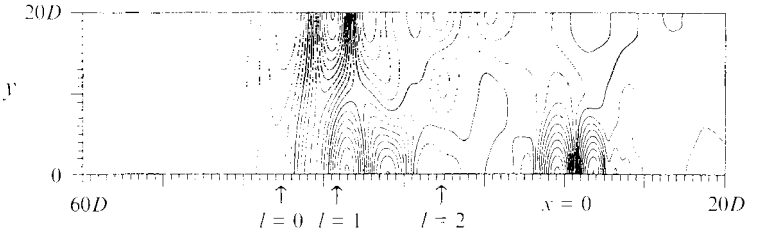

FIGURE 13. Contours of $A(x, y, t)$ obtained from the solution of the Navier–Stokes equations when $F = 0.6$ (linearly stratified Boussinesq flow, $Ut/D = 80$). The interval of the contour is $\Delta A = 0.002D$.

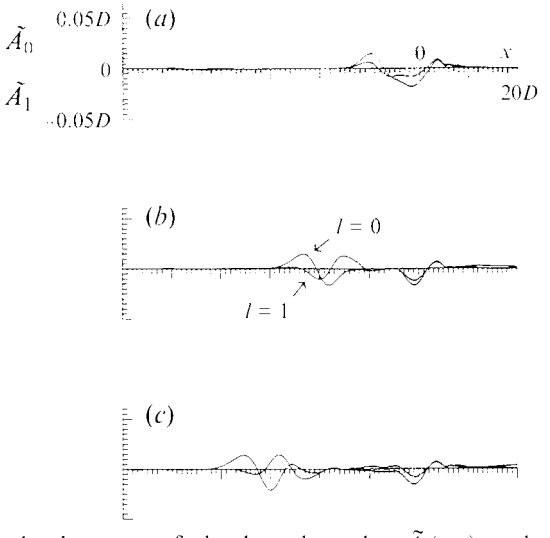

FIGURE 14. Time development of the lateral modes $\tilde{A}_0(x, t)$ and $\tilde{A}_1(x, t)$ in the solution of the Navier–Stokes equations when $F = 0.6$ (linearly stratified Boussinesq flow): (*a*) $Ut/D = 20$; (*b*) $Ut/D = 50$; (*c*) $Ut/D = 80$.

case. Figure 14 shows that the propagation speeds of modes $l = 0$ and $l = 1$ also have clear differences and this causes the two-dimensionalization of the upstream wave. By assuming

$$\rho \propto \mathrm{e}^{\mathrm{i}(kx-\omega t)} \cos(l\pi y/W) \sin(n\pi z/D) \tag{4.8}$$

in the linearized equations for linearly stratified Boussinesq fluid, we can derive a dispersion relation and the corresponding group velocity as

$$\omega = N\left(\frac{k^2+(l\pi/W)^2}{k^2+(l\pi/W)^2+(n\pi/D)^2}\right)^{\frac{1}{2}} \tag{4.9}$$

and

$$C_g = \frac{\partial\omega}{\partial k} = \frac{Nk(n\pi/D)^2}{(k^2+(l\pi/W)^2)^{\frac{1}{2}}(k^2+(l\pi/W)^2+(n\pi/D)^2)^{\frac{1}{2}}}. \tag{4.10}$$

The maximum group velocity occurs when

$$k = \left(\frac{1}{3}\frac{l\pi}{W}\right)^{\frac{1}{2}}\left[-\frac{l\pi}{W}+\left\{4\left(\frac{l\pi}{W}\right)^2+3\left(\frac{n\pi}{D}\right)^2\right\}^{\frac{1}{2}}\right]^{\frac{1}{2}}. \tag{4.11}$$

At time $Ut/D = 80$, the difference in the position of the foremost wave of modes

$l = 0$ and $l = 1$, obtained by substituting (4.11) into (4.10) ($n = 1$, $F = 0.6$, $W = 20D$) is $7.9D$. The wavelength of the foremost wave of mode $l = 1$ estimated by (4.11) is $11.9D$. These values are consistent with figure 14. Because the upstream wave in this case is sinusoidal and not similar to the Boussinesq solitary wave, abnormal reflection similar to the Mach reflection does not occur. We know that the nonlinear correction of the linear wave speed is small in the case of two-dimensional linearly stratified Boussinesq fluid. This would be applicable also to the three-dimensional fluid. Therefore, although the propagation speed is consistent with the prediction of the linear theory, this does not mean directly that the generation of upstream waves is described by the linearized equations.

5. Conclusions

We have found that the three-dimensional waves excited by an obstacle near resonance in nearly two-layer flow are described qualitatively by the fKP or the fEKP equation. In the process of the two-dimensionalization of the upstream wave, it was found that abnormal reflection similar to the Mach reflection of a Boussinesq solitary wave plays an important role. The phenomenon could not be explained by the difference in the group velocity of the lateral mode of the linear wave.

In the subcritical flow of the nearly two-layer fluid, similar two-dimensionalization of the upstream wave occurred. Again, the process was explained by the abnormal reflection of the wave at the sidewall, because the upstream wave again had a profile similar to the Boussinesq solitary wave.

In the case of linearly stratified Boussinesq flow, the two-dimensionalization of the upstream wave could be explained by the difference in the group velocity of the lateral mode of the linear wave, because the upstream wave had a sinusoidal structure and the abnormal reflection that is typical to the Boussinesq solitary waves could not occur. However, this does not directly mean that the generation of upstream waves can be described by linear theory because the nonlinear correction of the linear-wave speed would be very small in analogy with the results for two-dimensional waves.

REFERENCES

AKYLAS, T. R. 1984 On the excitation of long nonlinear waves by a moving pressure distribution. *J. Fluid Mech.* **141**, 455–466.

BAINES, P. G. 1977 Upstream influence and Long's model in stratified flows. *J. Fluid Mech.* **82**, 147–159.

BAINES, P. G. 1979 Observations of stratified flow over two-dimensional obstacles in fluid of finite depth. *Tellus* **31**, 351–371.

CASTRO, I. P. & SNYDER, W. H. 1988 Upstream motions in stratified flow. *J. Fluid Mech.* **187**, 487–506.

COLE, S. L. 1987 Transient waves produced by a moving pressure distribution. *Q. Appl. Maths* **45**, 51–58.

ERTEKIN, R. C. 1984 Soliton generation by moving disturbances in shallow water: Theory, computation and experiment. PhD dissertation, University of California, Berkeley.

ERTEKIN, R. C. & QIAN, Z. M. 1990 Numerical grid generation and upstream waves for ships in restricted waters. In *Proc. 5th Intl Conf. on Numerical Ship Hydrodynamics, Hiroshima, September 25–28, 1989* pp. 421–437 (ed. K.-H. Mori). Washington DC: National Academy Press.

ERTEKIN, R. C., QIAN, Z. M. & WEHAUSEN, J. V. 1990 Upstream solitons and wave resistance. In *Proc. Symp. to Honour T. Y. Wu, Cal. Ins. of Tech., August 17–18, 1989*. Published in *Engineering Science, Fluid Dynamics* (ed. G. T. Yates), pp. 29–44. World Scientific.

ERTEKIN, R. C., WEBSTER, W. C. & WEHAUSEN, J. V. 1984 Ship-generated solitons. In *Proc. 15th Symp. Naval Hydrodyn., Hamburg*, pp. 347–364. Washington, DC: National Academy of Sciences.

ERTEKIN, R. C., WEBSTER, W. C. & WEHAUSEN, J. V. 1986 Waves caused by a moving disturbance in a shallow channel of finite width. *J. Fluid Mech.* **169**, 275–292.

FUNAKOSHI, M. 1980 Reflection of obliquely incident solitary waves. *J. Phys. Soc. Japan* **49**, 2371–2379.

GREEN, A. E. & NAGHDI, P. M. 1976*a* Directed fluid sheets. *Proc. R. Soc. Lond.* A **347**, 447–473.

GREEN, A. E. & NAGHDI, P. M. 1976*b* A derivation of equations for wave propagation in water of variable depth. *J. Fluid Mech.* **78**, 237–246.

GRIMSHAW, R. 1990 Resonant flow of rotating fluid past an obstacle: The general case. *Stud. Appl. Maths.* **83**, 249–269.

GRIMSHAW, R. H. J. & SMITH, N. 1986 Resonant flow of a stratified fluid over topography. *J. Fluid Mech.* **169**, 429–464.

GRIMSHAW, R. & YI, Z. 1991 Resonant generation of finite-amplitude waves by the flow of a uniformly stratified fluid over topography. *J. Fluid Mech.* **229**, 603–628.

HANAZAKI, H. 1989*a* Drag coefficient and upstream influence in three-dimensional stratified flow of finite depth. *Fluid Dyn. Res.* **4**, 317–332.

HANAZAKI, H. 1989*b* Upstream advancing columnar disturbances in two-dimensional stratified flow of finite depth. *Phys. Fluids* A **1**, 1976–1987.

HANAZAKI, H. 1991 Upstream-advancing nonlinear waves in an axisymmetric resonant flow of rotating fluid past an obstacle. *Phys. Fluids* A **3**, 3117–3120.

HANAZAKI, H. 1992 A numerical study of nonlinear waves in a transcritical flow of stratified fluid past an obstacle. *Phys. Fluids* A **4**, 2230–2243.

HANAZAKI, H. 1993*a* Upstream-advancing nonlinear waves excited in an axisymmetric transcritical flow of rotating fluid. *Phys. Fluids* A **5**, 568–577.

HANAZAKI, H. 1993*b* On the nonlinear internal waves excited in the flow of a linearly stratified Boussinesq fluid. *Phys. Fluids.* A **5**, 1201–1205.

KATSIS, C. & AKYLAS, T. R. 1987 On the excitation of long nonlinear water waves by a moving pressure distribution. Part 2. Three-dimensional effects. *J. Fluid Mech.* **177**, 49–65.

KAWAMURA, T., TAKAMI, H. & KUWAHARA, K. 1986 Computation of high Reynolds number flow around a circular cylinder with surface roughness. *Fluid Dyn. Res.* **1**, 145–162.

LEE, S. J. & GRIMSHAW, R. H. J. 1990 Upstream-advancing waves generated by three-dimensional moving disturbances. *Phys. Fluid* A **2**, 194–201.

LEE, S. J., YATES, G. T. & WU, T. Y. 1989 Experiments and analysis of upstream-advancing solitary waves generated by moving disturbances., *J. Fluid Mech.* **199**, 569–593.

MA, H. & TULIN, M. P. 1993 Experimental study of ship internal waves: the supersonic case. *J. Offshore Mech. Arctic Engng.* **115**, 16–22.

MELVILLE, W. K. 1980 On the Mach reflection of a solitary wave. *J. Fluid Mech.* **98**, 285–297.

MELVILLE, W. K. & HELFRICH, K. R. 1987 Transcritical two-layer flow over topography. *J. Fluid Mech.* **178**, 31–52.

MILES, J. W. 1977*a* Obliquely interacting solitary waves. *J. Fluid Mech.* **79**, 157–169.

MILES, J. W. 1977*b* Resonantly interacting solitary waves. *J. Fluid Mech.* **79**, 171–179.

MILES, J. W. 1979 On internal solitary waves. *Tellus* **31**, 456–462.

MILOH, T., TULIN, M. P. & ZILMAN, G. 1993 Dead-water effects of a ship moving in stratified seas. *J. Offshore Mech. Arctic Engng* **115**, 105–110.

PEDERSEN, G. 1988 Three-dimensional waves patterns generated by moving disturbances at transcritical speeds. *J. Fluid Mech.* **196**, 39–63.

PERROUD, P. H. 1957 The solitary wave reflection along a straight vertical wall at oblique incidence. PhD thesis, University of California, Berkeley.

SMYTH, N. F. 1988 Dissipative effects on the resonant flow of a stratified fluid over topography. *J. Fluid Mech.* **192**, 287–312.

TANAKA, M. 1993 Mach reflection of a large-amplitude solitary wave. *J. Fluid Mech.* **248**, 637–661.

THAMES, F. C., THOMPSON, J. F., MASTIN, C. W. & WALKER, R. L. 1977 Numerical solutions for

viscous and potential flow about arbitrary two-dimensional bodies using body-fitted coordinate systems. *J. Comput. Phys.* **24**, 245–273.

TOMASSON, G. G. & MELVILLE, W. K. 1991 Flow past a constriction in a channel: a modal description. *J. Fluid Mech.* **232**, 21–45.

TULIN, M. P. & MILOH, T., 1991 Ship internal waves in a shallow thermocline: The supersonic case. In *18th Symp. Naval Hydrodynamics, Ann Arbor, MI*, pp. 567–581. Washington DC: National Academy Press.

WU, T. Y. 1981 Long waves in ocean and coastal waters. *J. Engng Mech. Div. ASCE* **107**, 501–522.

ZHU, J., WU, T. Y. & YATES, G. T. 1986 Generation of internal runaway solitons by moving disturbances. In *Proc. 16th Symp. on Naval Hydrodynamics*,(ed W. C. Webster), pp. 186–198. Washington DC: National Academy Press.

ZHU, J., WU, T. Y. & YATES, G. T. 1987 Internal solitary waves generated by moving disturbances. In *Proc 3rd Intl Symp. on Stratified Flows, February, Pasadena* (ed. E. L. List and G. H. Jirka), pp. 74–83. ASCE.